Fe XVIII–XXIV Kβ Inner-Shell Absorption Lines in the X-Ray Spectra of Neutron Star and Black Hole Binaries with XRISM

Masahiro TSUJIMOTO[1,2)]*, Daiki MIURA[1,2)], Hiroya YAMAGUCHI[1,2)], Ehud BEHAR[3)], Chris DONE[4)], María DÍAZ TRIGO[5)], Chamani M. GUNASEKERA[6)], Peter A. M. VAN HOOF[7)], Stefano BIANCHI[8)], Maryam DEHGHANIAN[9)], Gary J. FERLAND[9)]

[1)] *JAXA, ISAS, Sagamihara, Kanagawa 252-5210, Japan*
[2)] *The University of Tokyo, Bunkyo-ku, Tokyo 113-0033, Japan*
[3)] *Department of Physics, Technion, Haifa 3200003, Israel*
[4)] *Department of Physics, Durham University, Durham DH1 3LE, UK*
[5)] *ESO, 85748 Garching bei München, Germany*
[6)] *STSci, Baltimore, MD 21218, USA*
[7)] *Royal Observatory of Belgium, 1180 Brussels, Belgium*
[8)] *Università degli Studi Roma Tre, Rome, 00146 Lazio, Italy*
[9)] *University of Kentucky, Lexington, KY 40506, USA*

(Received 9 August 2025 / Accepted 13 October 2025)

The advent of the X-ray microcalorimeter spectrometer *Resolve* onboard the XRISM space telescope opened a new era for high-resolution X-ray spectroscopy of astrophysical plasmas. Many spectral features were newly detected, including the Kα and Kβ inner-shell transition lines of mildly ionized (F- to Li-like) Fe at 6–8 keV in the spectra of X-ray binaries and active galactic nuclei. The widely used atomic databases contain information on the Kα but not Kβ lines of these ions. We conducted the atomic structure calculation using `FAC` to derive the Fe Kα and Kβ lines and verified the result against ground experiments and other calculations of the Fe Kα lines. We then implemented the Fe Kβ lines in a radiative transfer code (`Cloudy`) and compared the synthesized and observed spectra with XRISM. A reasonably good agreement was obtained between the observation and the *ab initio* calculations. This exemplifies the need to expand the atomic databases to interpret astrophysical spectra.

Keywords: atomic structure calculation, radiative transfer calculation, astrophysical plasma, X-ray spectroscopy

DOI: 10.1585/pfr.21.2401002

1. Introduction

The advent of the *Resolve* instrument [1, 2] onboard the X-Ray Imaging and Spectroscopy Mission (XRISM) [3] opened a new era of high-resolution (4.5 eV FWHM at 5.9 keV [4]) X-ray spectroscopy in astrophysical plasmas. It is based on non-dispersive X-ray microcalorimetry [5] as opposed to the previous high-resolution X-ray spectrometers based on dispersive technologies [6–8] and excels in energy resolution, throughput, low background, timing accuracy, and bandpass at $\gtrsim 2$ keV.

Many spectral features were newly detected. One of them is the series of Fe Kα ($n = 2 \rightarrow 1$) and Fe Kβ ($n = 3 \rightarrow 1$) inner-shell excitation absorption features by mildly-ionized (F- to Li-like) Fe, respectively, in the 6.4–7.0 and 7.3–7.9 keV band (Fig. 1). These lines are observed in active galactic nuclei and X-ray binaries, which accrete matter into the gravitational potential of the compact objects (black holes and

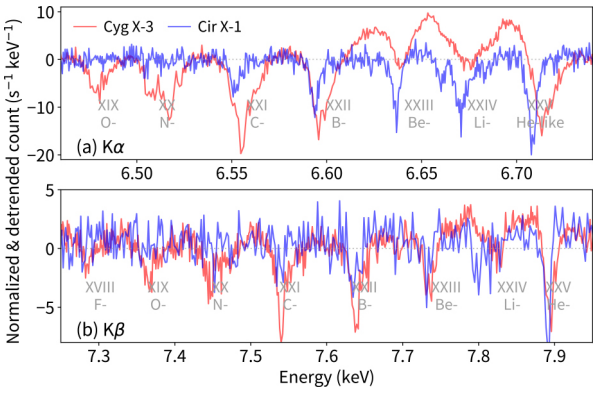

Fig. 1. XRISM X-ray spectra (continuum-subtracted and normalized) of Cyg X-3 [9] and Cir X-1 [10] for the (a) Fe Kα and (b) Kβ features of different charge states.

*Corresponding author's e-mail: tsujimoto.masahiro@jaxa.jp

This article is based on the presentation at the Joint Conference of the 22nd International Conference on Atomic Processes in Plasmas (APiP 2025) and 1st NIFS Conference on Atomic and Molecular Processes in Plasmas.

neutron stars; BH and NS). The released energy is dissipated into heat and is cooled radiatively. The intense radiation ionizes and accelerates matter around them, forming outflows of photo-ionized plasmas. This is one of the common mechanisms for the circulation of matter in the Universe. The Fe K absorption lines are useful probes of such outflows because of the large cosmic abundance of Fe and the high enough energy of the lines to penetrate the interstellar extinction.

What we need to interpret the observed spectra are (i) the atomic data of the transitions and (ii) the radiative transfer (RT) calculation to synthesize X-ray spectra under non-local thermodynamic equilibrium (NLTE) conditions. The atomic databases such as `AtomDB` [11, 12], `Chianti` [13], `OpenADAS` [14], `XSTARDB` [15], and the NIST atomic database [16]) and the RT codes such as `XSTAR` [17], `Cloudy` [18], and `SPEX` [19, 20] are widely used for astrophysical plasmas. We can constrain the physical properties of plasmas by comparing observed and synthesized spectra. This approach is generally established and applies to many lines, but not the Kβ lines of mildly ionized Fe due to the lack of relevant information in popular atomic databases. Though they were calculated earlier [21], only `Chianti` has the Fe Kβ transition entries for Fe XXIV now. Considering the ubiquity and utility of the Kβ lines observed with a high signal-to-noise ratio, this needs to be addressed urgently.

This study is one of such attempts. Our approach is to conduct the *ab initio* atomic structure calculation using a general-purpose code (Sec. 2.1). We verify the result against ground measurements and other calculations of the Fe Kα lines and extrapolate them to the Kβ lines (Sec. 2.2). We run the *ab initio* RT calculation by adding the Fe Kβ data thus obtained (Sec. 3) and compare the synthesized and observed spectra with XRISM (Sec. 4).

2. Atomic Structure Calculation

2.1 Calculation

We used the `FAC` (Flexible Atomic Code) version 1.1.5 [22] code for the atomic structure calculation. The code provides a general-purpose, fully relativistic numerical solver of the Dirac equation with a central field potential. In general, the jj coupling scheme is used in the relativistic structure calculations, while the LS coupling scheme is used in the atomic databases. The conversion from jj to LS coupling was performed using a routine in another structure calculation code `GRASP` [23].

We calculated the following inner-shell Kα and Kβ transitions for the Li- to F-like Fe:

Li-like 2s or 2p → 1s $2s^i\ 2p^{2-i}$ or 1s $2s^i\ 2p^{1-i}$ nl
Be-like $2s^2$ or 2s2p → 1s $2s^i\ 2p^{3-i}$ or 1s $2s^i\ 2p^{2-i}$ nl
B-like $2s^22p$ or $2s2p^2$ → 1s $2s^i\ 2p^{4-i}$ or 1s $2s^i\ 2p^{3-i}$ nl
C-like $2s^22p^2$ or $2s2p^3$ → 1s $2s^i\ 2p^{5-i}$ or 1s $2s^i\ 2p^{4-i}$ nl
N-like $2s^22p^3$ or $2s2p^4$ → 1s $2s^i\ 2p^{6-i}$ or 1s $2s^i\ 2p^{5-i}$ nl
O-like $2s^22p^4$ or $2s2p^5$ → 1s $2s^i\ 2p^{7-i}$ or 1s $2s^i\ 2p^{6-i}$ nl
F-like $2s^22p^5$ or $2s2p^6$ → 1s $2s^i\ 2p^{8-i}$ or 1s $2s^i\ 2p^{7-i}$ nl

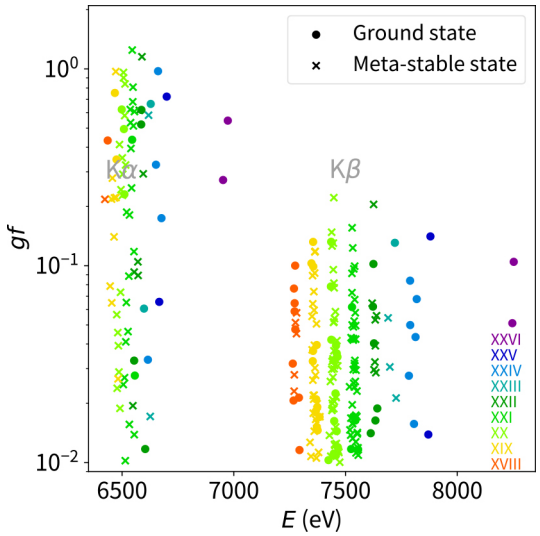

Fig. 2. Scatter plot of the line energy (E) and the weighted oscillator strengths (gf) of the Fe Kα and Kβ transitions calculated with FAC. Different symbols are used for the transitions from the ground or a metastable state. Different colors are used for different ionization stages.

where $n \in \{3, 4\}$, $i \in \{0, 1, 2\}$, $l \in \{\mathrm{s, p, d}\}$ ($n = 3$) or $\{\mathrm{s, p, d, f}\}$ ($n = 4$). Among them, we selected single-excitation and electric-dipole transitions from the ground state (GS) or a metastable state (MS) of the same quantum number n with the GS. The initial states are the following.

Li-like $2s\ ^2S_{1/2}$
Be-like $2s^2\ ^1S_0$, $2s2p\ ^3P_0$ (43), $^3P_2$ (58)
B-like $2s^22p\ ^2P_{1/2}$, $^2P_{3/2}$ (15)
C-like $2s^22p^2\ ^3P_0$, $^3P_1$ (9), $^3P_2$ (15), $^1D_2$ (30), $^1S_0$ (46)
N-like $2s^22p^3\ ^4S_{3/2}$, $^2D_{3/2}$ (18), $^2D_{5/2}$ (23), $^2P_{1/2}$ (33), $^2P_{3/2}$ (41)
O-like $2s^22p^4\ ^3P_2$, $^3P_0$ (9), $^3P_1$ (11), $^1D_2$ (22), $^1S_0$ (41)
F-like $2s^22p^5\ ^2P_{3/2}$, $^2P_{1/2}$ (13)

The excitation energy in eV is given in parentheses for the MS above GS, all of which are low enough to be collisionally excited from the predominant GS in the plasma with a temperature of ∼ 1 MK. We calculated the energy E (eV), the A coefficient (s^{-1}), and the weighted oscillator strength (gf) of these transitions (Fig. 2). The total number of strong ($gf > 10^{-2}$) Kα/Kβ transitions are 4/6 (Li), 4/4 (Be), 11/14 (B), 23/47 (C), 20/55 (N), 11/40 (O), and 2/14 (F-like).

2.2 Verification

The energies of the Fe Kα inner-shell transitions are well measured in ground experiments [24–26] and calculated in theories [27–31]. We compared our results with some of them in Fig. 3. The deviation of the `FAC` calculation from a ground experiment is within ± 1.5 eV (67 km s^{-1}), which is comparable to another calculation result [27] and typical uncertainty in energy determination with *Resolve* for mildly-ionized Fe features [10]. The mean deviation is 0 eV. We therefore do not apply any correction to match the `FAC` results, including the Fe Kβ transitions.

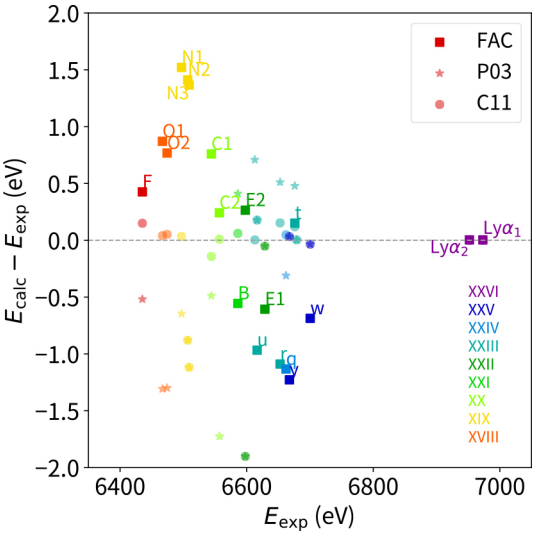

Fig. 3. Scatter plot of the Fe Kα line energy of the FAC calculation (this work), Palmeri *et al.* (2003; P03) [27], and `Chianti` version 11.0 [13] (C11) against a ground experiment [25]. The line labels follow [25].

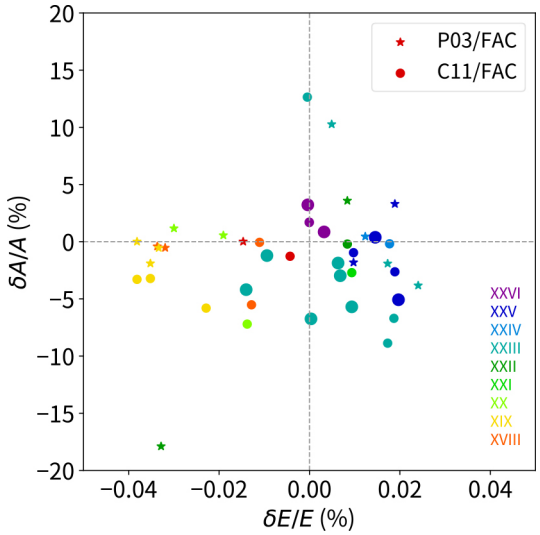

Fig. 4. Scatter plot of relative E and the A value of the Fe Kα and Kβ (respectively in smaller and larger symbols) between Palmeri *et al.* (2003; P03) [27] and `Chianti` version 11 [13] (C11) against the `FAC` calculation (this work).

We also compared the E and A values of the `FAC` calculation against another calculation [27] and the `Chianti` database [13] in Fig. 4. We estimate the systematic uncertainty of $\sim 5\%$ in A and 0.05% in E for the Kα (H- to F-like) and Kβ (H- to Li-like) lines. We anticipate a comparable level of systematics for the other Fe Kβ lines.

3. Radiative Transfer Calculation

Plasmas around BH and NS are considered to be in photoionized equilibrium. RT codes calculate the balances between heating/cooling for the temperature, ionization/recombination for the charge population, and excitation/deexcitation for the level population consistently with the external radiation field. All relevant radiative and collisional interactions need to be considered. By solving the radiative transfer equation, we obtain the synthesized spectra of both the direct and reprocessed emission. The direct emission is from the BH and NS through the plasma, in which absorption features are imprinted upon otherwise featureless continuum emission. The reprocessed emission is composed of the electron-scattered emission of the direct emission, and recombination and deexcitation emission of ions in the plasma.

We used `Cloudy` (c25 release candidate [32]), which is one of the most widely used RT codes in astrophysics. It adopts the two-stream solver in one-dimensional setup with the line escape probability approximation without solving the diffusion across wavelengths. Intensive efforts have been made in recent years to make it suitable for high-resolution spectroscopy with X-ray microcalorimeters [33–36], and it is indeed applied to XRISM data [37, 10, 38]. We used `Chianti` [13] for the atomic database among several options with the method in [39]. Although being most complete, it still lacks the Fe Kβ inner-shell transition of Be- to F-like Fe. We supplemented them with our results in Sec. 2.

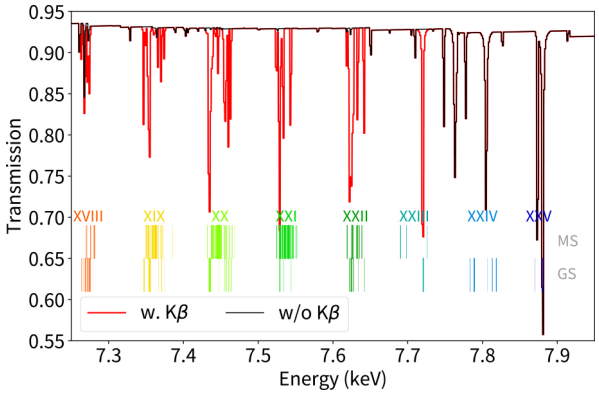

Fig. 5. Transmission through the plasma of $n = 10^{12.0}$ cm^{-3}, $N_{\rm H} = 10^{22.5}$ cm^{-2}, and $\xi = 10^{2.8}$ erg cm s^{-1} calculated with `Cloudy` by adding the Be- to F-like Fe Kβ transitions (red) compared to the original (black). Line energies of the Kβ transitions are shown by vertical lines separately for those from the GS or a MS with a width proportional to their $\log(gf)$ value.

We ran `Cloudy` for a grid of three parameters (n, $N_{\rm H}$, and ξ). A plane parallel (slab) geometry was assumed with a constant density of n (cm^{-3}) and no turbulence velocity over the slab, and a column density of $N_{\rm H}$ (cm^{-2}) across the slab. The incident radiation is characterized by the ionization degree $\xi \equiv L_{1-1,000}/nr_{\rm in}^2$ (erg cm s^{-1}), in which $L_{1-1,000}$ is the incident luminosity integrated over 1–1,000 Ryd [40] and $r_{\rm in}$ is the distance from the incident source to the illuminated surface of the slab. The incident radiation has the spectral shape of a multi-color disk blackbody emission [41] with an innermost temperature of 2 keV, which is typical among X-ray binaries. Figure 5 shows an example of the synthesized transmitted spectrum.

4. Comparison to Observations

We now compare the synthesised and observed spectra. We used the XRISM observations of Cyg X-3 (sequence number 300065010) made on 2024 March 24–25 for an integration time of 66.6 ks and Cir X-1 (201036010) on 2025 February 13–15 for 81.5 ks. Cyg X-3 is a binary of a putative BH and a high-mass star with an orbital period of 4.8 hour [42], and almost seven whole rotations were covered by XRISM. Cir X-1 is a binary of a NS and a low-mass star with a period of 16.6 day [43], and a part of a whole rotation (stable phase [44]) was covered. Both are at a distance of $\sim$ 10 kpc from the Sun and have an X-ray luminosity of $\sim 10^{37}$ erg s^{-1}.

Figure 1 shows their *Resolve* spectra in the Fe Kα and Kβ bands. Cyg X-3 [9] shows both absorption and emission features stemming from the direct and reprocessed emission, respectively. They have different Doppler velocity shifts (-530 and 130 km s^{-1}) forming a typical P Cygni profile. This is a direct consequence of the velocity structure made by the stellar wind of the high-mass star. The lines are broadened by $\sim$ 600 km s^{-1} (12 eV), which is much larger than the thermal ($\sim$ 3 eV) and natural ($\sim$ 0.3 eV) broadening. Cir X-1, on the other hand, shows only the absorption features. This is because direct emission overwhelms the reprocessed emission, and thus the emission lines are almost invisible. The absorption lines are Doppler-shifted and broadened less than Cyg X-3 but more than the thermal and natural broadening.

We fitted Cir X-1 spectrum with a spectral model consisting of a multi-color disk blackbody attenuated by the plasma transmission (Fig. 5) and the interstellar extinction. Lines are shifted for the bulk Doppler motion. A parameter set ($\log \xi$ = 3.0 erg cm s^{-1}, $\log n$ = 14.0 cm^{-3}, $\log N_{\rm H}$ = 22.5 cm^{-2}) gave a good description overall in both the Fe Kα (Fig. 6a) and Kβ (Fig. 6b) bands. Major observed features are qualitatively explained, though with some non-negligible deviations. These deviations provide new constraints on the plasma, such as the v, n, and $N_{\rm H}$ structures as a function of ξ or r once the atomic data are verified by cross-comparing different calculations and verification with ground experiments, as was done for Fe Kα in [20, 27, 25].

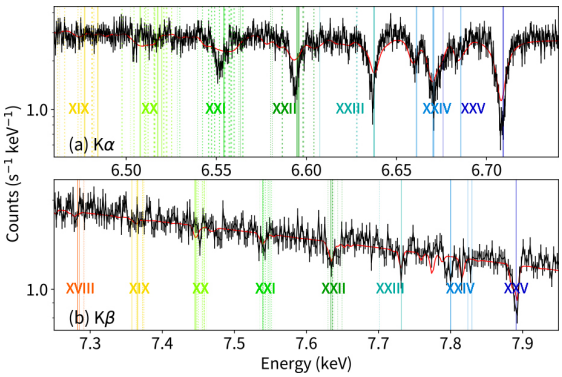

Fig. 6. Best-fit RT model (red lines) and the XRISM spectra (black) of Cir X-1. The transitions from the GS and MS are given in solid and dotted lines with the energy shifted blue-ward by the best-fit Doppler velocity of 425 km s^{-1}.

Acknowledgements

Daiji Kato at NIFS reviewed and improved the manuscript. Gediminas Gaigalas at Vilnius University and Wenxian Li at CAS provided updates of the JJ2LSJ routine in the GRASP package. Many participants in the APiP2025 meeting provided useful comments. This work was supported by the JSPS Core-to-Core Program (grant number: JPJSCCA20220002) and made use of the JAXA's high-performance computing system JSS3.

[1] R.L. Kelley *et al.*, JATIS **11**, 042026 (2025).
[2] Y. Ishisaki *et al.*, JATIS **11**, 042023 (2025).
[3] M.S. Tashiro *et al.*, PASJ **77**, S1 (2025).
[4] F.S. Porter *et al.*, JATIS **11**, 042016 (2025).
[5] D. McCammon *et al.*, J. Appl. Phys. **56**, 1263 (1984).
[6] C.R. Canizares *et al.*, PASP **117**, 1144 (2005).
[7] A.C. Brinkman *et al.*, Proc. of SPIE **4012**, 81 (2000).
[8] J.W. den Herder *et al.*, A&A **365**, L7 (2001).
[9] XRISM Collaboration, ApJL **977**, L34 (2024).
[10] M. Tsujimoto *et al.*, PASJ **77**, S72 (2025).
[11] R.K. Smith *et al.*, ASP Conf. Ser. **247**, 161 (2001).
[12] A.R. Foster *et al.*, AIP Conf. Proc. **1811**, 190005 (2017).
[13] G. del Zanna *et al.*, ApJ **909**, 38 (2021).
[14] H.P. Summers, The ADAS User Manual 2.6 (2004).
[15] C. Mendoza *et al.*, Atoms **9**, 12 (2021).
[16] A. Kramida *et al.*, NIST Atomic Spectra Database 5.12 (2024).
[17] Y.K. Ko and T.R. Kallman, ApJ **431**, 273 (1994).
[18] G.J. Ferland *et al.*, RMAA **53**, 385 (2017).
[19] J. Kaastra *et al.*, *11th Colloq. on UV and X-ray Spectroscopy of Astrophysical and Laboratory Plasmas* 411 (1996).
[20] M. Mehdipour *et al.*, A&A **596**, A65 (2016).
[21] E. Behar and H. Netzer, ApJ **570**, 165 (2002).
[22] M.F. Gu, CJP **86**, 675 (2008).
[23] C. Froese Fischer *et al.*, CPC **237**, 184 (2019).
[24] V.A. Yerokhin and A. Surzhykov, JPCRD **47**, 023105 (2018).
[25] J. K. Rudolph *et al.*, PRL **111**, 103002 (2013).
[26] N. Hell *et al.*, arXiv 2506.17106 (2025).
[27] P. Palmeri *et al.*, A&A **403**, 1175 (2003).
[28] P. Palmeri *et al.*, A&A **410**, 359 (2003).
[29] M.A. Bautista *et al.*, A&A **403**, 339 (2003).
[30] M.A. Bautista *et al.*, A&A **418**, 1171 (2004).
[31] T.R. Kallman *et al.*, ApJS **155**, 675 (2004).
[32] C.M. Gunasekera *et al.*, RNAAS **7**, 246 (2023).
[33] F. Camilloni *et al.*, RNAAS **5**, 149 (2021).
[34] P. Chakraborty *et al.*, ApJ **901**, 68 (2020).
[35] P. Chakraborty *et al.*, ApJ **901**, 69 (2020).
[36] P. Chakraborty *et al.*, ApJ **912**, 26 (2020).
[37] C.M. Gunasekera et al., A&A **694**, L13 (2025).
[38] Y. Mochizuki *et al.*, PASJ **77**, S63 (2025).
[39] C.M. Gunasekera *et al.*, Astronomy **1**, 255 (2022).
[40] C.B. Tarter *et al.*, ApJ **156**, 943 (1969).
[41] K. Mitsuda *et al.*, PASJ **36**, 741 (1984).
[42] D.R. Parsignault *et al.*, NPhS **239**, 123 (1972).
[43] L.J. Kaluzienski *et al.*, ApJ **208**, L71 (1976).
[44] M. Tominaga *et al.*, ApJ **958**, 52 (2023).